Supplementary Information for

Development of a thermodynamic approach to assist the control of the precipitation of hydroxyapatites and associated calcium phosphates in open systems

Corentin Reynaud,[1] Cyril Thomas,[1] Sandra Casale,[1] Sophie Nowak[2] and Guylène Costentin[1]*

[1] *Sorbonne Université, CNRS, Laboratoire de Réactivité de Surface (LRS), 4 place Jussieu, 75005 Paris, France*

[2] *Plateforme Rayons X, UFR de Chimie, Université Paris Diderot, Paris, France*

*E-mail: guylene.costentin@sorbonne-universite.fr

This document includes:

S1 - pH control

pH meter operation. The syntheses were carried out using an automated reactor controlling the pH during the addition step. In order to check the correct operation of the pH probe, the pH of the medium was modelled during the temperature rise step for the P → Ca synthesis. The reactor initially at 20 °C contained, 200 mL of a calcium solution (0.22 mol/L) adjusted to about pH 10 by adding a few drops of concentrated ammonia ($C_0 \approx 0.002$ mol/L in the reactor). This solution was heated up to 80 °C under stirring (400 rpm) and a significant decrease in pH of about 1.5 unit was observed (Figure S1A). The acid-base reaction which imposes the pH during this temperature rise step is:

$$NH_{3(aq)} + H_2O_{(l)} = NH_{4(aq)}^{+} + OH_{(aq)}^{-} \quad \text{(Eq. S1)}$$

associated with the following equilibrium constant:

$$K^o = \frac{K_w}{K_a(NH_4^+/NH_3)} \quad \text{(Eq. S2)}$$

with K_w the autoprotolysis equilibrium constant of water and $K_a(NH_4^+/NH_3)$ the acidity constant associated with the NH_4^+/NH_3 acid-base couple The pH of the medium can be expressed as a function of the equilibrium constants K_w and $K_a(NH_4^+/NH_3)$ as well as the C_0 ammonia concentration in the reactor initially introduced at 20 °C. The change in pH during the temperature rise results from the temperature dependence of the equilibrium constants.[1,2] The theoretical model

was found to fit reasonably well the experimental data, thus confirming the correct operation of the pH meter at 80 °C (Figure S1A).

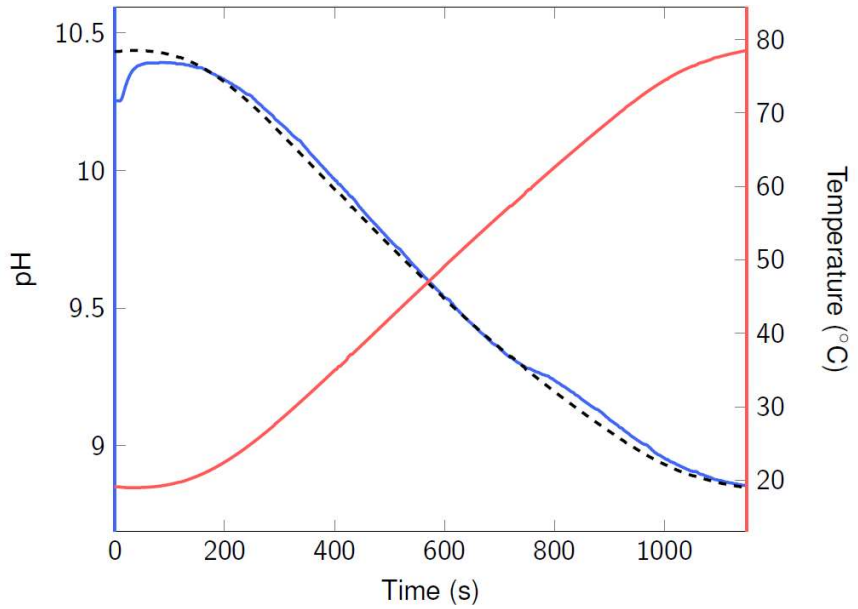

Figure S1A. Experimental (blue trace) and modelled (dashed black trace) pH evolution in the reactor during the temperature rise step from 20 to 80 °C (orange trace) (Table 2, sample 1).

Synthesis pH **profile.** The synthesis of calcium phosphates is particularly sensitive to the pH of the reaction medium. The automated reactor allows for the control of this parameter, as illustrated in Figure S1B showing a characteristic pH profile recorded for an experiment carried out at pH 9.0 and 80 °C. During the temperature rise (Figure S1B, step A), the pH was found to decrease because of the influence of the temperature on the acid base equilibrium (*pH meter operation* section). The pH was then rapidly readjusted to pH 9.0 by adding concentrated ammonia drop by drop (Figure S1B, step B). The calcium or phosphate solution is then gradually added into the reactor. The pH could be reasonably kept constant by the addition of concentrated ammonia controlled by the automated reactor (Figure S1B, step C and Figure S1C) in the course of the addition of the solutions of phosphate or calcium precursors. A white precipitate is instantaneously formed during that step as the first drops of solutions of precursors are added for all experiments performed at pH 9.0 and 6.5, whereas the formation of such a precipitate was slightly delayed for the syntheses performed at pH 4.2 (Table 2). These observations are in line with the minimal concentrations $[Ca^{2+}]_{min}$ and $[P]_{min}$ calculated from the methodology developed in this study implying that, at pH 4.2, the concentration of Ca^{2+} (Ca → P) or $H_xPO_4^{(3-x)-}$ (P → Ca) ions into the reactor by one drop, is not sufficient to induce the precipitation of any CaP contrary to what occurs for the syntheses

performed at pH 6.5 and 9.0 (Figure 3 **A**, **B**). For the synthesis performed at pH 9.0 and 80 °C (Table 2, sample 1), once the precipitation step was completed, few amounts (approximately 1 mL) of ammonia were required to keep the pH constant due to the need in counterbalancing the gaseous NH_3 released during the maturation step.

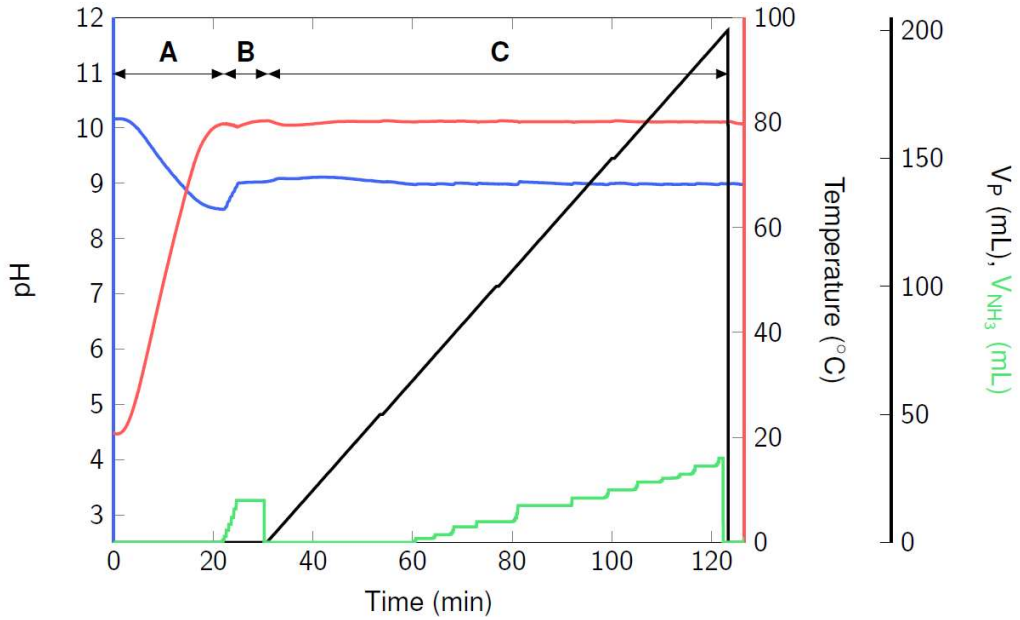

Figure S1B. Temperature profile (red trace), pH profile (blue trace) and volumes added of phosphate precursor (black trace) and ammonia (green trace) solutions into the reactor in the case of a P → Ca synthesis performed at 80 °C at pH 9.0 (Table 2, samples 2).

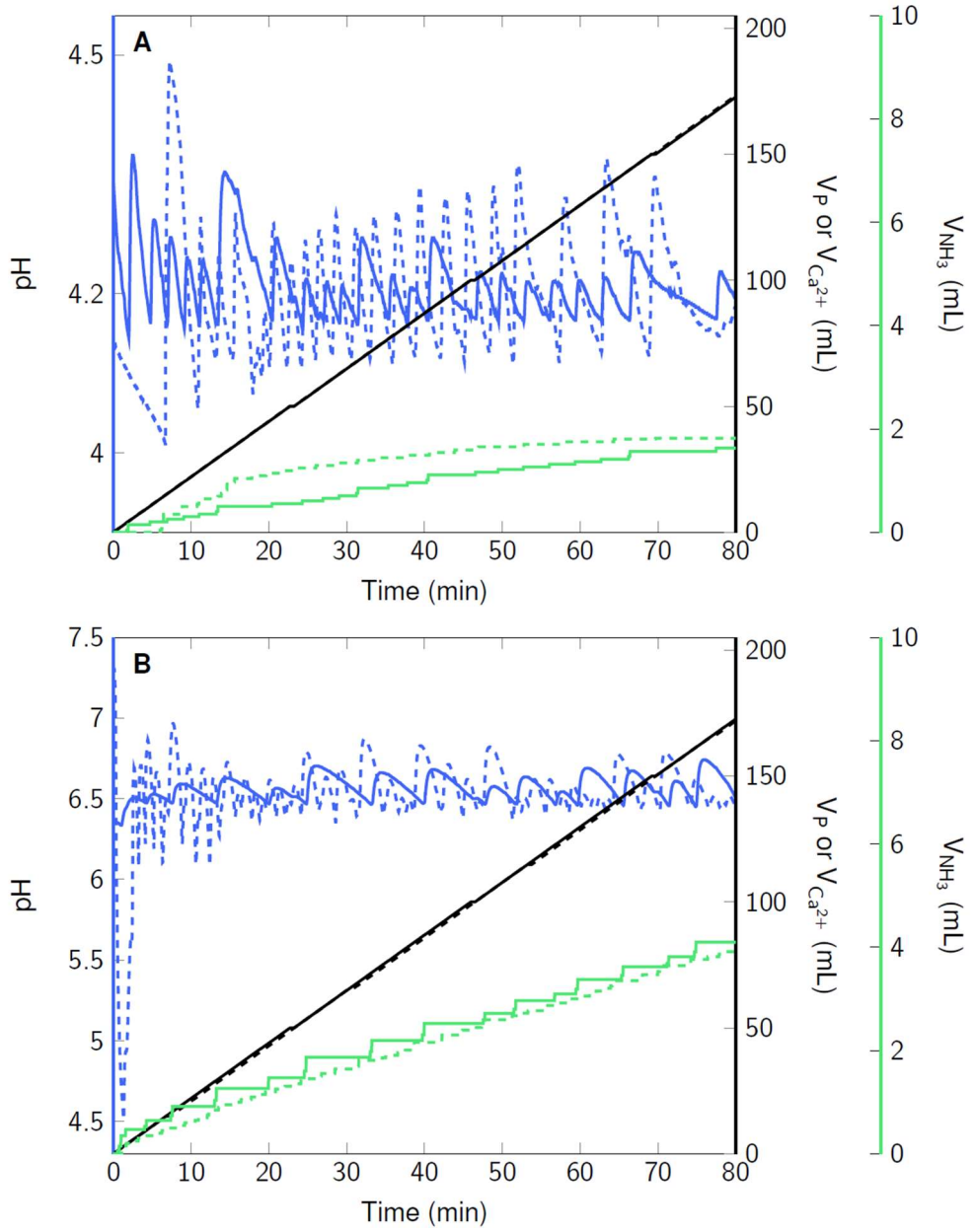

Figure S1C. Comparison of the pH stability (blue traces) in the reactor during the addition step at 80 °C and pH 4.2 (**A**) or 6.5 (**B**) between the P → Ca (Table 2, sample 5, dashed line) and Ca → P (Table 2, sample 7, solid line) synthesis routes. The pH control parameters are: mixing time = 12 s, minimum pH deviation = 0.02 and maximum pH rate = 0.3 pH unit/min. Note that the pH is easier to maintain constant when the calcium solution is added gradually into the reactor (Ca → P route) compared to that of the phosphate solution (P → Ca route).

S2 - Indexation of the XRD lines and Raman bands of CaPs

Both XRD and Raman spectroscopy techniques were complementary used to identify the nature of calcium phosphate(s) obtained after washing/drying steps as well as their crystallinity and the origins of the substoichiometry of HAp (Tables S2A and S2B).

Table S2A. XRD assignment of the diffraction lines below 40 ° for crystalline calcium phosphates: HAp (reference card n° 00-009-0432, ICDD), OCP (reference card n° 00-026-1056, ICDD), DCPD (reference card n° 00-009-0077) and DCPA (reference card n° 00-009-0080). The relative intensity (Int.) of each (h k l) diffraction line is indicated as a percentage of the most intense diffraction line.

HAp			**OCP**			**DCPD**			**DCPA**		
2θ (°)	(hkl)	Int. (%)	2θ (°)	(hkl)	Int. (%)	2θ (°)	(hkl)	Int. (%)	2θ (°)	(hkl)	Int. (%)
			4.72	(010)	100						
			9.44	(020)	15						
10.82	(100)	12	9.77	(110)	13	11.68	(020)	100			
			14.51	(1-20)	2				13.12	(010)	14
			16.04	(-101)	8						
			16.35	(021)	2				16.31	(100)	4
			17.00	(1-11)	1						
			17.37	(-111)	4	17.98	(-111)	2	17.76	(0-11)	4
			18.41	(1-31)	2						
18.78	(110)	4	18.84	(0-31)	2						
			18.99	(040)	1						
			19.65	(031)	3				19.80	(011)	2
			19.75	(-121)	3				20.26	(-101)	4
			20.67	(131)	2	20.93	(021)	100	20.79	(1-20)	4
21.82	(200)	10	21.60	(230)	2						
			22.67	(1-40)	5				22.04	(101)	4
22.90	(111)	10	22.91	(201)	4						
			23.01	(-201)	3						
			23.48	(041)	3	23.39	(040)	8			
			23.74	(221)	5	23.71	(130)	< 1			
			24.30	(-211)	10	24.50	(-131)	2	24.03	(1-21)	4
25.35	(201)	2	25.49	(231)	8				25.58	(-121)	14

25.88	(002)	40	25.87	(2-21)	17						
			26.00	(002)	20				26.43	(020)	70
			26.36	(-221)	6				26.59	(2-20)	75
			26.91	(-1-51)	8				26.75	(2-10)	16
			27.18	(1-50)	8				27.00	(002)	10
			27.78	(250)	3						
28.13	(102)	12	28.04	(241)	2						
			28.47	(-1-22)	5				28.49	(-1-21)	20
28.97	(201)	18	28.61	(-112)	3				28.77	(0-12)	6
			29.21	(0-32)	5	29.26	(041)	75	29.90	(-221)	2
			29.60	(330)	3				30.19	(-112)	100
			30.31	(-122)	5				30.41	(-102)	35
			30.66	(-151)	4	30.51	(-221)	50	30.68	(2-11)	4
			31.10	(251)	10				31.02	(021)	8
			31.55	(260)	33	31.30	(-112)	10	31.17	(111)	4
31.77	(211)	100	31.70	(2-41)	32	31.97	(200)	2	31.44	(012)	2
32.20	(112)	60	32.18	(-1-42)	15				32.38	(1-30)	10
			32.59	(331)	12				32.48	(2-30)	20
32.90	(300)	60	33.06	(042)	8				32.89	(102)	35
			33.52	(070)	17	33.54	(150)	4			
34.05	(202)	25	33.97	(1-61)	12	33.82	(131)	4			
			34.24	(3-30)	7	34.15	(220)	50			
			34.38	(2-22)	7	34.43	(-202)	30			
			34.92	(-161)	5	35.11	(002)	4	34.73	(2-31)	4
35.48	(301)	6	35.25	(-1-71)	4	35.42	(060)	2	35.42	(-122)	4
			36.10	(-2-51)	2	35.60	(-132)	4	35.91	(0-22)	16
			36.27	(052)	3				36.06	(-1-12)	2
			36.53	(1-70)	2	36.90	(-241)	14	36.76	(201)	2
			38.02	(180)	2	37.10	(022)	16	37.26	(-212)	2
			38.52	(271)	3				38.25	(2-22)	4
39.20	(212)	8	39.06	(-302)	2				39.04	(120)	10
			39.65	(361)	2				39.37	(2-12)	2
			39.76	(-1-81)	2	39.71	(061)	4			
39.82	(310)	20	39.89	(062)	2						

Table S2B. Raman shift (cm^{-1}) of PO_4^{3-} and HPO_4^{2-} groups of (CD)HAp, ACP, OCP, DCPD and DCPA reported in earlier works.[3–6]

	(CD)HAp	ACP	OCP	DCPD	DCPA
$\nu_3(PO_4)$ or $\nu_3(HPO_4)$ stretch	1077 1064 1057 1048 1041 1034 1029	1118 1050	1112 (HPO_4^{2-} hydrated layer) 1079 (PO_4^{3-} and HPO_4^{2-}) 1052 (PO_4^{3-}) 1048 (PO_4^{3-}) 1036 (PO_4^{3-}) 1027 (PO_4^{3-})	1132 1119 1079 1061	1131 1094
$\nu_1(PO_4)$ or $\nu_1(HPO_4)$ stretch	1011 (HPO_4^{2-} CDHAp) 941–961	 951	1011 (HPO_4^{2-}) 1005 (HPO_4^{2-}) 966 (PO_4^{3-}) 959 (PO_4^{3-})	986	988
$\nu(P—OH)$ stretch	920 (CDHAp) 879 (CDHAp)		916 (apatite layer) 874 (hydrated layer)	 878	900
$\nu_4(PO_4)$ or $\nu_4(HPO_4)$ stretch	614 607 591 580	 594	619 (PO_4^{3-}) 609 (PO_4^{3-}) 591 (PO_4^{3-} and HPO_4^{2-}) 577 (PO_4^{3-} and HPO_4^{2-}) 556 (PO_4^{3-}) 523 (PO_4^{3-})	 588 525	 588 574 563
$\nu_2(PO_4)$ or $\nu_2(HPO_4)$ stretch	448 433	451 419	451 (PO_4^{3-}) 427 (PO_4^{3-}) 409 (HPO_4^{3-}) 353 (HPO_4^{2-} hydrated layer)	 411 381	 420 394

S3 - XRF calibration traces

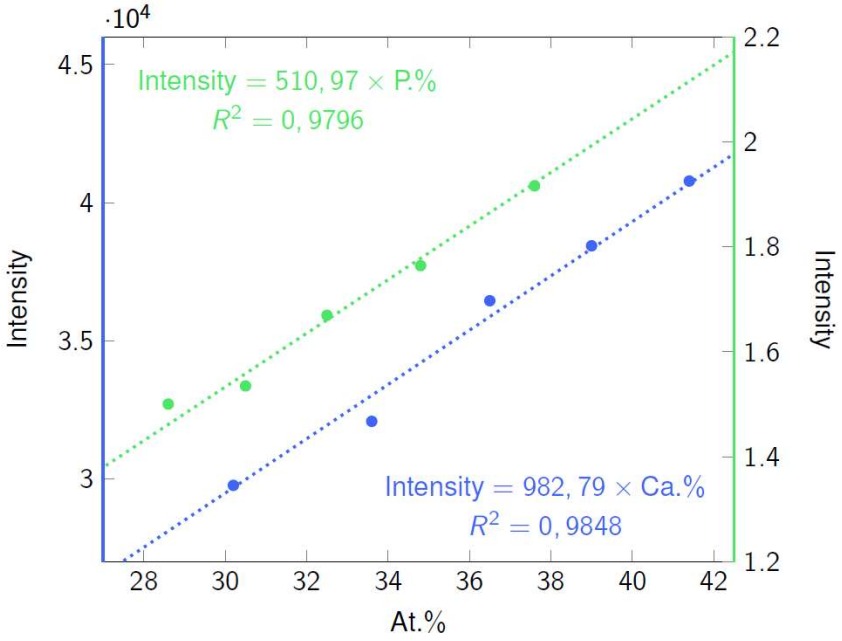

Figure S3. XRF calibration traces for the quantification of calcium (blue) and phosphorous (green). The dots represent the results of XRF analyses on beads of mechanical reference mixtures (see *Materials and Methods*). The dotted lines are the linear regressions used in the study to determine the Ca/P ratios of the synthesized CaPs.

S4 - Apparent solubility of CaPs

The phosphate and hydrogen phosphate groups constitutive of CaPs confer them a solubility in aqueous medium that is greatly influenced by the pH of the latter. The apparent solubility product $K_{s,\,app}^{CaP}$ associated with each calcium phosphate mineral is considered in order to analyze the influence of the acid-base equilibria on their dissolution in water. This temperature-dependent parameter is expressed from the solubility constants K_s^{CaP} of the CaPs and the acidity constants K_{ai} associated with the various phosphate species (Table 1).

In the case of the HAp crystalline phase, the dissolution-precipitation equilibrium in a buffered medium can be defined as:

$$\mathrm{Ca_5(PO_4)_3OH_{(s)}} + (9x + 6y + 3z + q)\mathrm{H_3O^+_{(aq)}} = 5\ \mathrm{Ca^{2+}_{(aq)}} + 3x\ \mathrm{H_3PO_{4(aq)}} + 3y\ \mathrm{H_2PO^-_{4(aq)}} + 3z\ \mathrm{HPO^{2-}_{4(aq)}} + 3n\ \mathrm{PO^{3-}_{4(aq)}} + (1-q)\ \mathrm{HO^-_{(aq)}} + (9x + 6y + 3z + 2q)\ \mathrm{H_2O_{(l)}} \qquad \text{(Eq. S3)}$$

where x, y, z and n stand for the molar fractions associated with $\mathrm{H_3PO_4}$, $\mathrm{H_2PO_4^-}$, $\mathrm{HPO_4^{2-}}$ and $\mathrm{PO_4^{3-}}$ entities, respectively, and q and $1-q$ the molar fractions of oxonium and hydroxide ions,

respectively. The dissolution equilibrium is associated with an apparent equilibrium constant $K_{s,\,app}^{HAp}$ which can be expressed according to:

$$K_{s,\,app}^{HAp} = \frac{K_s^{HAp}}{K_{a1}^{3x} K_{a2}^{3(x+y)} K_{a3}^{3(x+y+z)} K_w^q} \qquad \text{(Eq. S4)}$$

where K_w is the autoprotolysis constant of water. Detailed demonstration for obtention of Eq. S4 is provided below. Due to the dependence of the molar fractions x, y, z, n and q on the pH at the equilibrium (Figure S4A and Eqs. S16– S19), the apparent solubility product is also a function of the latter, *i.e.* $K_{s,\,app}^{HAp} = f(\mathrm{pH}_{eq})$. Hence, as commonly written in a strongly basic medium where $x \simeq y \simeq z \simeq q \simeq 0$ and $n \simeq 1$ (Figure S4A and Figure S4B), the dissolution equilibrium comes down to:

$$\mathrm{Ca_5(PO_4)_3OH_{(s)}} = 5\ \mathrm{Ca^{2+}_{(aq)}} + 3\ \mathrm{PO^{3-}_{4(aq)}} + \mathrm{HO^{-}_{(aq)}} \qquad \text{(Eq. S5)}$$

with

$$K_{s,\,app}^{HAp} = K_s^{HAp} = a(\mathrm{Ca^{2+}})_{eq}^5\, a(\mathrm{PO_4^{3-}})_{eq}^3\, a(\mathrm{HO^-})_{eq} \qquad \text{(Eq. S6)}$$

where $a(\mathrm{i})_{eq}$ is the activity of the species i at the equilibrium and $K_s^{HAp} = 10^{-58.6}$ at 37 °C.[7] Likewise, the pH dependence of the apparent solubility product can be expressed for each CaPs as developed below. For all of them, it appears that the lower the pH of the medium solution at the equilibrium, the higher the apparent solubility (Figure S4A). Such a significant increase in the solubility of CaPs in an acidic medium is accounted for by the speciation diagram of the phosphate species in solution. As the pH decreases, the protonation of the $\mathrm{PO_4^{3-}}$ and $\mathrm{HPO_4^{2-}}$ groups of the CaPs, into $\mathrm{HPO_4^{2-}}$, $\mathrm{H_2PO_4^-}$ and $\mathrm{H_3PO_4}$ species, leads to a shift of the dissolution-precipitation equilibria towards the dissolution of the CaPs (Figure S4A). Although the $K_{s,\,app}^{HAp}$ parameter is dependent on the temperature of the medium (Table 1), its evolution as a function of the pH_{eq}, is only slightly influenced in the 37–80 °C temperature range at atmospheric pressure (Figures S4A and S4B). This result reflects the weak influence of this parameter on the stability of CaPs in aqueous solution.

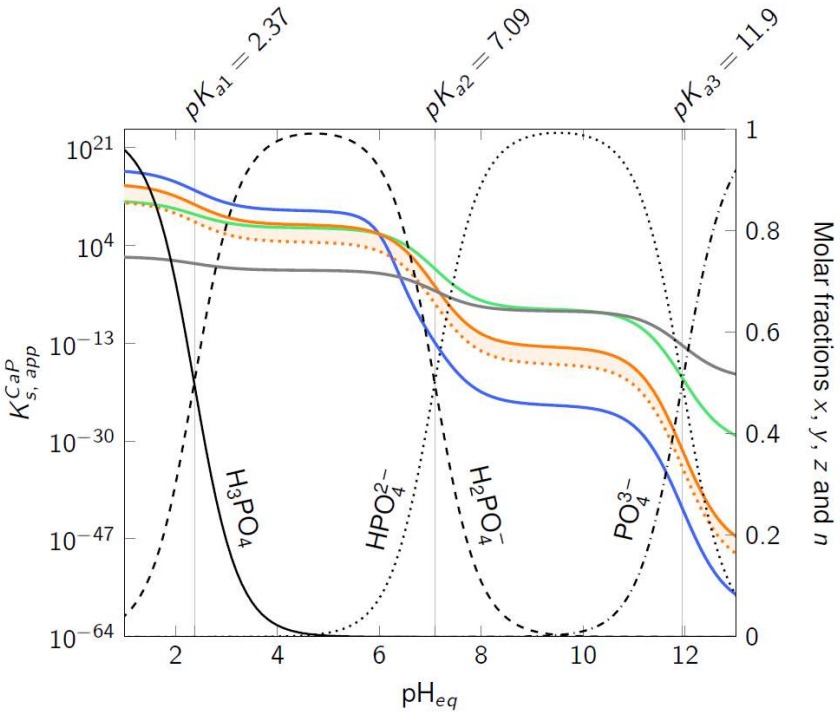

Figure S4A. Evolution of the apparent solubility product $K_{s,\,app}^{CaP}$ of HAp, ACP, OCP and DCPA as a function of the pH at the equilibrium at 80 °C. As the DCPD trace is almost superimposed with that of DCPA, it is not plotted in the figure for a readability reason. For OCP, due to the important uncertainty on the value of its solubility product at 80 °C (Table 1), the corresponding domain is highlighted in orange. The speciation of the phosphate species in aqueous solution at 80 °C: H_3PO_4 (x, solid line), $H_2PO_4^-$ (y, dashed line), HPO_4^{2-} (z, dotted line) and PO_4^{3-} (n, dotdashed line).

In the acidic domain, the DCPA mineral is the CaP with the lowest apparent solubility product, whereas HAp has the highest one (Figure S4A). The reverse situation is observed in the alkaline domain, with DCPA and HAp becoming the most and the least soluble CaPs, respectively. These observations are fully consistent with the numerous protocols reported in the literature that report on the formation of DCPA and HAp under acidic and neutral/basic conditions, respectively.[8,9] However, the $K_{s,\,app}^{CaP}$ parameter is not fully relevant to predict which CaP mineral will thermodynamically precipitate first under realistic operating synthesis conditions. In that respect, at a given pH in open systems (see *Materials and Methods*), the Ca/P ratio of these compounds (Table 1), varying from 1.00 (DCPD and DCPA) to 1.67 (HAp), needs to be taken into account.

The apparent solubility product $K_{s,\,app}^{CaP}$ of a specified CaP mineral was determined based on its solubility constant K_s^{CaP} and the equilibrium constants involving phosphate species (K_{ai}) and water (K_w) defined on Table 1. The computational method used is detailed in the case of hydroxyapatite. This mineral solubilizes in water according to Eq. S5.

Phosphate ions PO_4^{3-} are involved in the acid-base equilibrium:

$$HPO_{4(aq)}^{2-} + H_2O_{(l)} = PO_{4(aq)}^{3-} + H_3O_{(aq)}^{+} \quad \text{(Eq. S7)}$$

with

$$K_{a3} = \frac{a(PO_4^{3-})_{eq}\, a(H_3O^+)_{eq}}{a(HPO_4^{2-})_{eq}} \quad \text{(Eq. S8)}$$

The protonation of PO_4^{3-} ions allows the involvement of two other acid-base equilibria:

$$H_2PO_{4(aq)}^{-} + H_2O_{(l)} = HPO_{4(aq)}^{2-} + H_3O_{(aq)}^{+} \quad \text{(Eq. S9)}$$

with

$$K_{a2} = \frac{a(HPO_4^{2-})_{eq}\, a(H_3O^+)_{eq}}{a(H_2PO_4^{-})_{eq}} \quad \text{(Eq. S10)}$$

and

$$H_3PO_{4(aq)} + H_2O_{(l)} \;=\; H_2PO_{4(aq)}^{-} + H_3O_{(aq)}^{+} \quad \text{(Eq. S11)}$$

with

$$K_{a1} = \frac{a(H_2PO_4^{-})_{eq}\, a(H_3O^+)_{eq}}{a(H_3PO_4)_{eq}} \quad \text{(Eq. S12)}$$

Hydroxide ions are involved in the autoprotolysis equilibrium of water:

$$2\, H_2O_{(l)} \;=\; HO_{(aq)}^{-} + H_3O_{(aq)}^{+} \quad \text{(Eq. S13)}$$

with

$$K_w = a(H_3O^+)_{eq}\, a(HO^-)_{eq} \quad \text{(Eq. S14)}$$

No acid-base/complexation equilibrium involving Ca^{2+} cations was considered.

The apparent equilibrium constant $K_{s,\,app}^{HAp}$ can be expressed based on Eq. S4 as a function of the activity of the different species:

$$K_{s,\,app}^{HAp} = \frac{a(Ca^{2+})_{eq}^{5}\, a(PO_4^{3-})_{eq}^{3}\, a(HO^-)_{eq}}{K_{a1}^{3x} K_{a2}^{3(x+y)} \left(\frac{a(PO_4^{3-})_{eq}\, a(H_3O^+)_{eq}}{a(HPO_4^{2-})_{eq}}\right)^{3(x+y+z)} \left(a(H_3O^+)_{eq}\, a(HO^-)_{eq}\right)^{q}}$$

$$K_{s,\,app}^{HAp} = \frac{a(\mathrm{Ca^{2+}})_{eq}^{5} a(\mathrm{PO_4^{3-}})_{eq}^{3} a(\mathrm{HO^-})_{eq}^{1-q}}{K_{a1}^{3x}\left(\frac{a(\mathrm{HPO_4^{2-}})_{eq} a(\mathrm{H_3O^+})_{eq}}{a(\mathrm{H_2PO_4^-})_{eq}}\right)^{3(x+y)}\left(\frac{a(\mathrm{PO_4^{3-}})_{eq}}{a(\mathrm{HPO_4^{2-}})_{eq}}\right)^{3(x+y+z)} a(\mathrm{H_3O^+})_{eq}^{q+3(x+y+z)}}$$

$$K_{s,\,app}^{HAp} = \frac{a(\mathrm{Ca^{2+}})_{eq}^{5} a(\mathrm{PO_4^{3-}})_{eq}^{3} a(\mathrm{HO^-})_{eq}^{1-q} a(\mathrm{HPO_4^{2-}})_{eq}^{3z}}{K_{a1}^{3x}\left(\frac{1}{a(\mathrm{H_2PO_4^-})_{eq}}\right)^{3(x+y)} a(\mathrm{PO_4^{3-}})_{eq}^{3(x+y+z)} a(\mathrm{H_3O^+})_{eq}^{q+6(x+y)+3z}}$$

The speciation of phosphate species (Figures S4A and S4B) implies that at any pH the relation $x + y + z + n = 1$ is verified. The last equation simplifies as:

$$K_{s,\,app}^{HAp} = \frac{a(\mathrm{Ca^{2+}})_{eq}^{5} a(\mathrm{HO^-})_{eq}^{1-q} a(\mathrm{PO_4^{3-}})_{eq}^{3n} a(\mathrm{HPO_4^{2-}})_{eq}^{3z}}{\left(\frac{a(\mathrm{H_2PO_4^-})_{eq} a(\mathrm{H_3O^+})_{eq}}{a(\mathrm{H_3PO_4})_{eq}}\right)^{3x}\left(\frac{1}{a(\mathrm{H_2PO_4^-})_{eq}}\right)^{3(x+y)} a(\mathrm{H_3O^+})_{eq}^{q+6(x+y)+3z}}$$

$$K_{s,\,app}^{HAp} = \frac{a(\mathrm{Ca^{2+}})_{eq}^{5} a(\mathrm{HO^-})_{eq}^{1-q} a(\mathrm{PO_4^{3-}})_{eq}^{3n} a(\mathrm{HPO_4^{2-}})_{eq}^{3z} a(\mathrm{H_2PO_4^-})_{eq}^{3y}}{\left(\frac{1}{a(\mathrm{H_3PO_4})_{eq}}\right)^{3x} a(\mathrm{H_3O^+})_{eq}^{q+9x+6y+3z}}$$

Finally, the following equation is obtained:

$$K_{s,\,app}^{HAp} = \frac{a(\mathrm{Ca^{2+}})_{eq}^{5} a(\mathrm{HO^-})_{eq}^{1-q} a(\mathrm{PO_4^{3-}})_{eq}^{3n} a(\mathrm{HPO_4^{2-}})_{eq}^{3z} a(\mathrm{H_2PO_4^-})_{eq}^{3y} a(\mathrm{H_3PO_4^-})_{eq}^{3x}}{a(\mathrm{H_3O^+})_{eq}^{q+9x+6y+3z}} \quad \text{(Eq. S15)}$$

which accounts for the general dissolution equilibrium of HAp in a buffered medium (Eq. S3).

The parameters x, y, z, n and q are dependent on the pH at the equilibrium (Figures S4A and S4B) according to:

$$x = \frac{[\mathrm{H_3PO_4}]_{eq}}{[\mathrm{P}]_{tot}} \frac{1}{1 + \frac{K_{a1}}{10^{-\mathrm{pH}_{eq}}} + \frac{K_{a1}K_{a2}}{10^{-2\mathrm{pH}_{eq}}} + \frac{K_{a1}K_{a2}K_{a3}}{10^{-3\mathrm{pH}_{eq}}}} \quad \text{(Eq. S16)}$$

$$y = \frac{[\mathrm{H_2PO_4^-}]_{eq}}{[\mathrm{P}]_{tot}} = \frac{\frac{K_{a1}}{10^{-\mathrm{pH}_{eq}}}}{1 + \frac{K_{a1}}{10^{-\mathrm{pH}_{eq}}} + \frac{K_{a1}K_{a2}}{10^{-2\mathrm{pH}_{eq}}} + \frac{K_{a1}K_{a2}K_{a3}}{10^{-3\mathrm{pH}_{eq}}}} \quad \text{(Eq. S17)}$$

$$z = \frac{[\mathrm{HPO_4^{2-}}]_{eq}}{[\mathrm{P}]_{tot}} = \frac{\frac{K_{a1}K_{a2}}{10^{-2\mathrm{pH}_{eq}}}}{1 + \frac{K_{a1}}{10^{-\mathrm{pH}_{eq}}} + \frac{K_{a1}K_{a2}}{10^{-2\mathrm{pH}_{eq}}} + \frac{K_{a1}K_{a2}K_{a3}}{10^{-3\mathrm{pH}_{eq}}}} \quad \text{(Eq. S18)}$$

$$n = \frac{[\mathrm{PO_4^{3-}}]_{eq}}{[\mathrm{P}]_{tot}} = \frac{\frac{K_{a1}K_{a2}K_{a3}}{10^{-3\mathrm{pH}_{eq}}}}{1 + \frac{K_{a1}}{10^{-\mathrm{pH}_{eq}}} + \frac{K_{a1}K_{a2}}{10^{-2\mathrm{pH}_{eq}}} + \frac{K_{a1}K_{a2}K_{a3}}{10^{-3\mathrm{pH}_{eq}}}} \quad \text{(Eq. S19)}$$

$$q = \frac{10^{-\mathrm{pH}_{eq}}}{10^{-\mathrm{pH}_{eq}} + 10^{\mathrm{pH}_{eq}+\mathrm{p}K_w}} \quad \text{(Eq. S20)}$$

with $[\mathrm{P}]_{tot} = [\mathrm{H_3PO_4}]_{eq} + [\mathrm{H_2PO_4^-}]_{eq} + [\mathrm{HPO_4^{2-}}]_{eq} + [\mathrm{PO_4^{3-}}]_{eq}$ the total concentration in phosphate species.

The calculation of the apparent solubility product associated with the HAp mineral accounts for the influence of the pH on its solubility as $K_{s,\,app}^{HAp} = f(x, y, z, n, q) = f(\mathrm{pH}_{eq})$.

Similarly, the apparent solubility products associated with the other calcium phosphates (ACP, OCP, DCPD and DCPA) were determined. In the case of ACP, the dissolution equilibrium in a buffered medium is defined as:

$$\mathrm{Ca_3(PO_4)_{2(s)}} + (6x + 4y + 2z)\mathrm{H_3O^+_{(aq)}} = 3\,\mathrm{Ca^{2+}_{(aq)}} + 2x\,\mathrm{H_3PO_{4(aq)}} + 2y\,\mathrm{H_2PO^-_{4(aq)}} + 2z\,\mathrm{HPO^{2-}_{4(aq)}} + 2n\,\mathrm{PO^{3-}_{4(aq)}} + (6x + 4y + 2z)\,\mathrm{H_2O_{(l)}} \quad \text{(Eq. S21)}$$

It is associated with an apparent equilibrium constant $K_{s,\,app}^{ACP}$:

$$K_{s,\,app}^{ACP} = \frac{K_s^{ACP}}{K_{a1}^{2x} K_{a2}^{2(x+y)} K_{a3}^{2(x+y+z)}} \quad \text{(Eq. S22)}$$

In the case of OCP, the dissolution equilibrium in a buffered medium is defined as:

$$\mathrm{Ca_4HPO_4(PO_4)_2} \cdot \frac{5}{2}\mathrm{H_2O_{(s)}} + (9x + 6y + 3z - 1)\mathrm{H_3O^+_{(aq)}} = 4\,\mathrm{Ca^{2+}_{(aq)}} + 3x\,\mathrm{H_3PO_{4(aq)}} + 3y\,\mathrm{H_2PO^-_{4(aq)}} + 3z\,\mathrm{HPO^{2-}_{4(aq)}} + 3n\,\mathrm{PO^{3-}_{4(aq)}} + (9x + 6y + 3z + \frac{3}{2})\,\mathrm{H_2O_{(l)}} \quad \text{(Eq. S23)}$$

It is associated with an apparent equilibrium constant $K_{s,\,app}^{OCP}$:

$$K_{s,\,app}^{OCP} = \frac{K_s^{OCP}}{K_{a1}^{3x} K_{a2}^{3(x+y)} K_{a3}^{3(x+y+z-1)}} \quad \text{(Eq. S24)}$$

In the case of DCPD, the dissolution equilibrium in a buffered medium is defined as:

$$\mathrm{CaHPO_4} \cdot 2\mathrm{H_2O_{(s)}} + (2x + y - \mathrm{n} - 1)\mathrm{H_3O^+_{(aq)}} = \mathrm{Ca^{2+}_{(aq)}} + x\,\mathrm{H_3PO_{4(aq)}} + y\,\mathrm{H_2PO^-_{4(aq)}} + z\,\mathrm{HPO^{2-}_{4(aq)}} + n\,\mathrm{PO^{3-}_{4(aq)}} + (2x + y - \mathrm{n} + 2)\,\mathrm{H_2O_{(l)}} \quad \text{(Eq. S25)}$$

It is associated with an apparent equilibrium constant $K_{s,\,app}^{DCPD}$:

$$K_{s,\,app}^{DCPD} = \frac{K_s^{DCPD} K_{a3}^n}{K_{a1}^x K_{a2}^{x+y}} \qquad \text{(Eq. S26)}$$

Finally, in the case of DCPA, the dissolution equilibrium in a buffered medium is defined as:

$$\mathrm{CaHPO_{4(s)}} + (2x + y - \mathrm{n} - 1)\mathrm{H_3O^+_{(aq)}} = \mathrm{Ca^{2+}_{(aq)}} + x\ \mathrm{H_3PO_{4(aq)}}$$

$$+ y\ \mathrm{H_2PO^-_{4(aq)}} + z\ \mathrm{HPO^{2-}_{4(aq)}} + n\ \mathrm{PO^{3-}_{4(aq)}} + (2x + y - \mathrm{n})\ \mathrm{H_2O_{(l)}} \qquad \text{(Eq. S27)}$$

It is associated with an apparent equilibrium constant $K_{s,\,app}^{DCPA}$:

$$K_{s,\ app}^{DCPA} = \frac{K_s^{DCPA} K_{a3}^n}{K_{a1}^x K_{a2}^{x+y}} \qquad \text{(Eq. S28)}$$

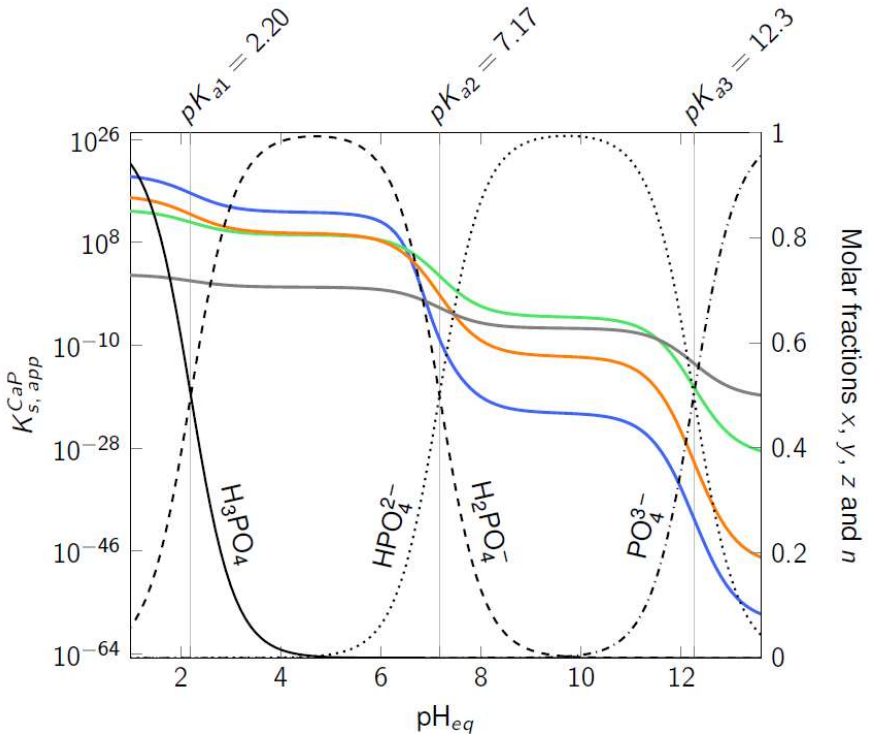

Figure S4B. Evolution of the apparent solubility product $K_{s,\,app}^{CaP}$ of HAp, ACP, OCP and DCPA as a function of the pH_{eq} at 37 °C. As the DCPD trace is almost superimposed with that of DCPA, it has not been plotted for a readability reason. Speciation of phosphate species in aqueous solution at 37 °C: $\mathrm{H_3PO_4}$ (x, solid line), $\mathrm{H_2PO_4^-}$ (y, dashed line), $\mathrm{HPO_4^{2-}}$ (z, dotted line) and $\mathrm{PO_4^{3-}}$ (n, dotdashed line).

S5 - Precipitation conditions of CaPs for the Ca → P and P → Ca synthesis routes

The thermodynamic approach developed in section I *Thermodynamic modelling of the precipitation of calcium phosphates in open systems* for the HAp material has been applied to

predict the conditions for the precipitation of ACP, OCP, DCPD and DCPA. Note that the criterion $Q \geq K_s$ (thermodynamic driving force) that was taken to estimate the precipitation conditions is the same as that commonly reported as $S \geq 1$, where S is the supersaturation of the solution. Indeed, for an ionic solid of stoichiometry ν, these different parameters are linked according to equation S29:

$$S = \left(\frac{Q}{K_s}\right)^{\frac{1}{\nu}} \quad \text{(Eq. S29)}$$

Following the Ca → P synthesis route, the different CaPs precipitate spontaneously at the beginning of the addition step if the concentration $[\mathrm{Ca^{2+}}]_{min}^{CaP}$ introduced into the reactor verifies:

$$[\mathrm{Ca^{2+}}]_{min}^{ACP} = \frac{1}{\gamma_{2\pm}}\left(\frac{K_s^{ACP}(c°)^5}{\gamma_{3\pm}^2[\mathrm{PO_4^{3-}}]_r^2}\right)^{\frac{1}{3}} \quad \text{(Eq. S30)}$$

$$[\mathrm{Ca^{2+}}]_{min}^{OCP} = \frac{1}{\gamma_{2\pm}}\left(\frac{K_s^{OCP}(c°)^8}{\gamma_{3\pm}^3[\mathrm{PO_4^{3-}}]_r^3\gamma_{\pm}[\mathrm{H_3O^+}]_r}\right)^{\frac{1}{4}} \quad \text{(Eq. S31)}$$

$$[\mathrm{Ca^{2+}}]_{min}^{DCPD} = \frac{K_s^{DCPD}(c°)^2}{\gamma_{2\pm}^2[\mathrm{HPO_4^{2-}}]_r} \quad \text{(Eq. S32)}$$

$$[\mathrm{Ca^{2+}}]_{min}^{DCPA} = \frac{K_s^{DCPD}(c°)^2}{\gamma_{2\pm}^2[\mathrm{HPO_4^{2-}}]_r} \quad \text{(Eq. S33)}$$

Following the P → Ca synthesis route, the different CaPs precipitate spontaneously at the beginning of the addition step if the concentration $[\mathrm{P}]_{min}^{CaP}$ introduced into the reactor verifies:

$$[\mathrm{P}]_{min}^{ACP} = \frac{1}{n\gamma_{3\pm}}\left(\frac{K_s^{ACP}(c°)^5}{\gamma_{2\pm}^3[\mathrm{Ca^{2+}}]_r^3}\right)^{\frac{1}{2}} \quad \text{(Eq. S34)}$$

$$[\mathrm{P}]_{min}^{OCP} = \frac{1}{n\gamma_{3\pm}}\left(\frac{K_s^{OCP}(c°)^8}{\gamma_{2\pm}^3[\mathrm{Ca^{2+}}]_r^4\gamma_{\pm}[\mathrm{H_3O^+}]_r}\right)^{\frac{1}{3}} \quad \text{(Eq. S35)}$$

$$[\mathrm{P}]_{min}^{DCPD} = \frac{K_s^{DCPD}(c°)^2}{z\gamma_{2\pm}^2[\mathrm{Ca^{2+}}]_r} \quad \text{(Eq. S36)}$$

$$[\mathrm{P}]_{min}^{DCPA} = \frac{K_s^{DCPA}(c^\circ)^2}{z\gamma_{2\pm}^2[\mathrm{Ca}^{2+}]_r} \qquad \text{(Eq. S37)}$$

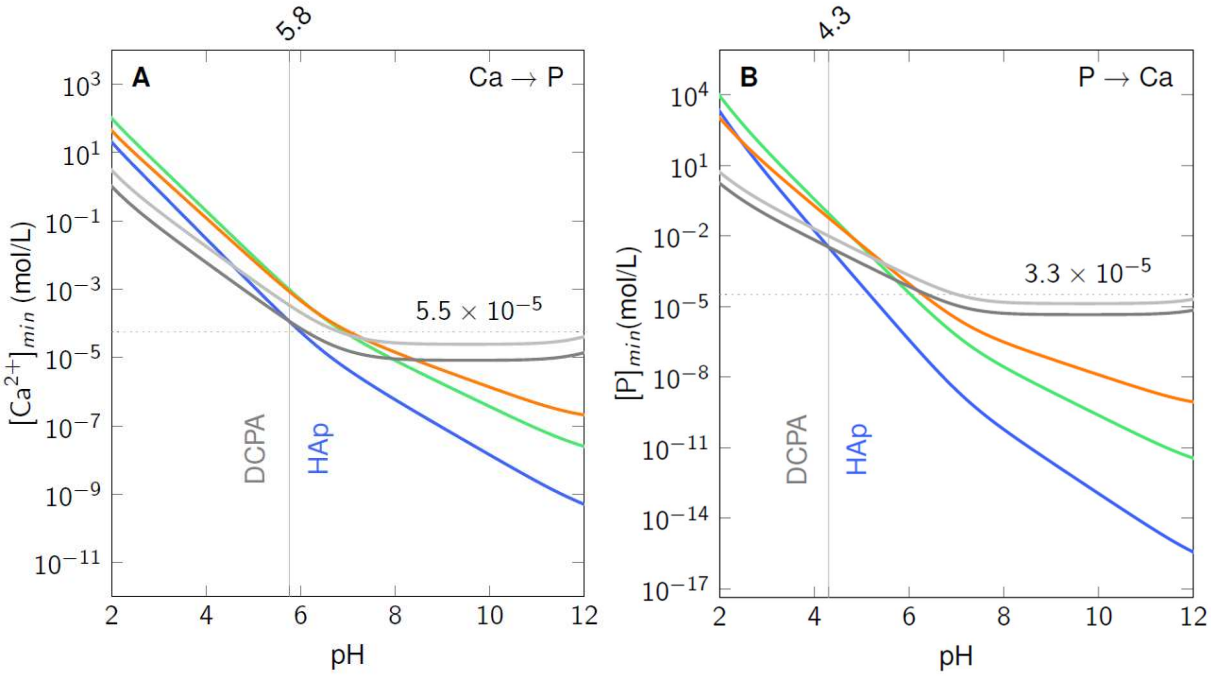

Figure S5A. Thermodynamic traces predicting the minimum concentration in precursor to be initially introduced into the reactor for both Ca → P (**A**) and P → Ca (**B**) routes in order to precipitate the different calcium phosphates HAp, ACP, OCP, DCPD and DCPA at 37 °C (modelling parameters: $[\mathrm{P}]_r = 0.13$ mol/L, and $[\mathrm{Ca}^{2+}]_r = 0.22$ mol/L). Specified concentrations of $[\mathrm{Ca}^{2+}] = 5.5 \times 10^{-5}$ mol/L and $[\mathrm{P}] = 3.3 \times 10^{-5}$ mol/L are those estimated in the reactor after one drop of the corresponding precursor is added (see *Materials and Methods*).

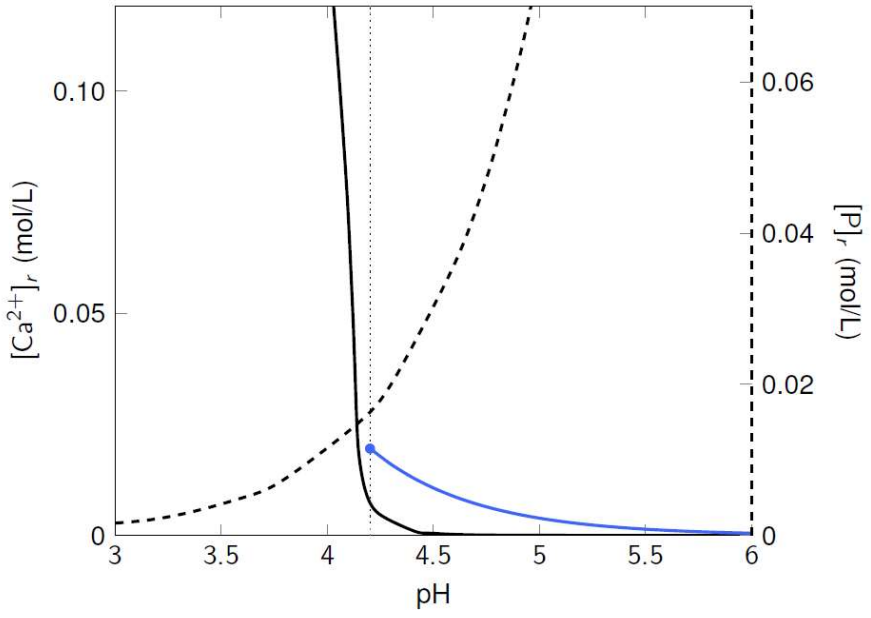

Figure S5B. Magnification of Figure 5 showing in blue, the concentrations in calcium ions and phosphate species at the end of the addition step considering a targeted final ratio $[Ca^{2+}]/[P]$ of 1.67 and assuming that the thermodynamic equilibrium is achieved. Note that the more acidic the reaction medium at the equilibrium, the greater the concentration of Ca^{2+} and $H_xPO_4^{(3-x)-}$ ions as discussed in Section I.

S6 - Low-angle diffractograms of HAp samples prepared at pH 6.5

The diffractograms of the samples prepared at pH 6.5 were acquired at low-angles to ascertain the absence of OCP in the corresponding samples (Figure S6).

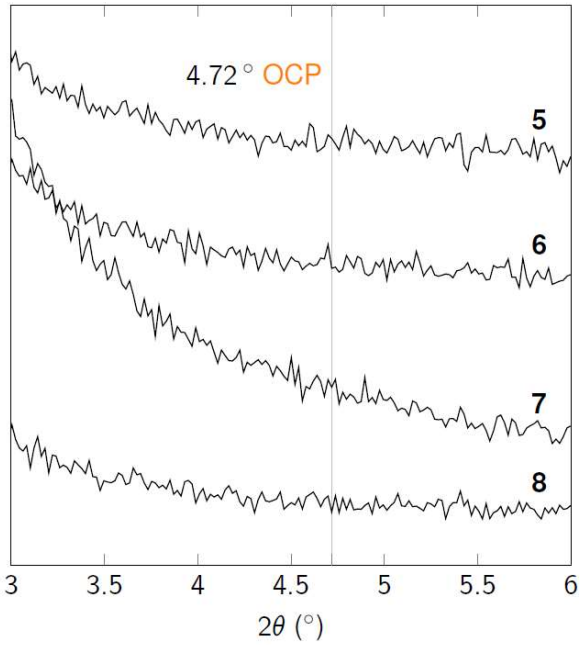

Figure S6. Low-angle XRD patterns of samples 5, 6, 7 and 8 prepared at pH 6.5 (Table 2).

S7 - DCPA hydrolysis into CDHAp during the washing step

Due to the slight acidity of the distilled water (pH ≈ 6.5) and the absence of phosphate ions, the DCPA formed in the reactor is susceptible to be hydrolyzed into HAp during the washing step (Figure S7). In that respect, the impact of the exposure time of DCPA to distilled water was investigated by comparing two procedures: centrifugation (precipitates exposed for ≈ 1 h to distilled water) and filtration on Büchner (precipitates exposed for ≈ 5 min to distilled water).

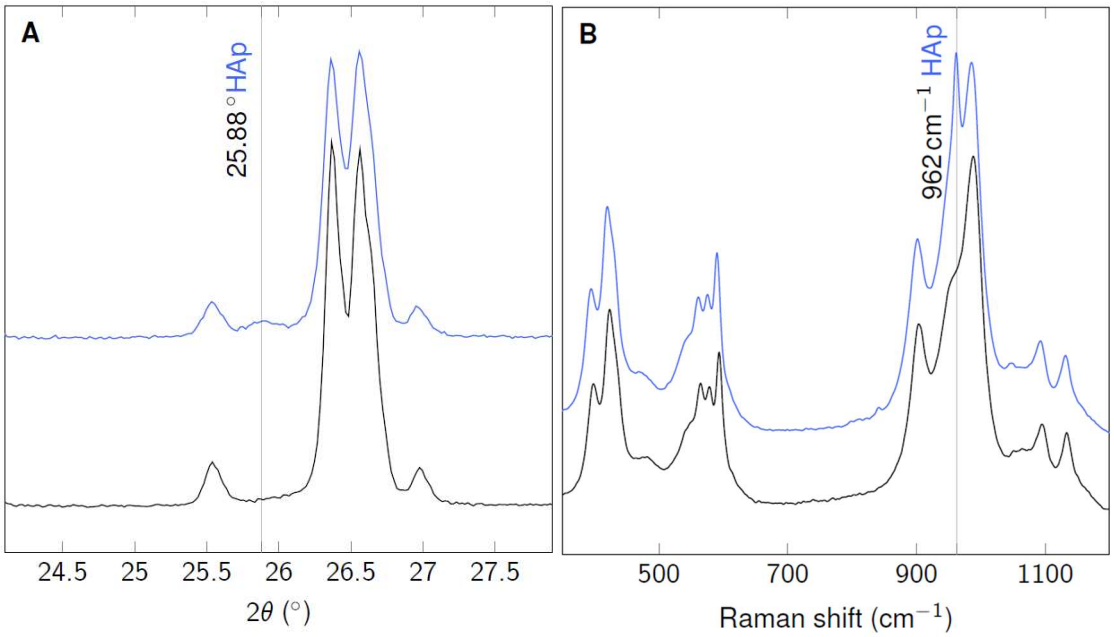

Figure S7. XRD patterns (**A**) and Raman spectra (**B**) of the samples prepared at pH 4.2 and 80 °C following the P → Ca route after recovering and washing promptly with distilled water on Büchner (black line) or by centrifugation (blue line, sample 11). The longer exposure of the sample in a slightly acidic medium when recovered by centrifugation compared to filtration on Büchner allow for more pronounced hydrolysis of DCPA into (CD)HAp in the precipitates.

S8 - Sample 13

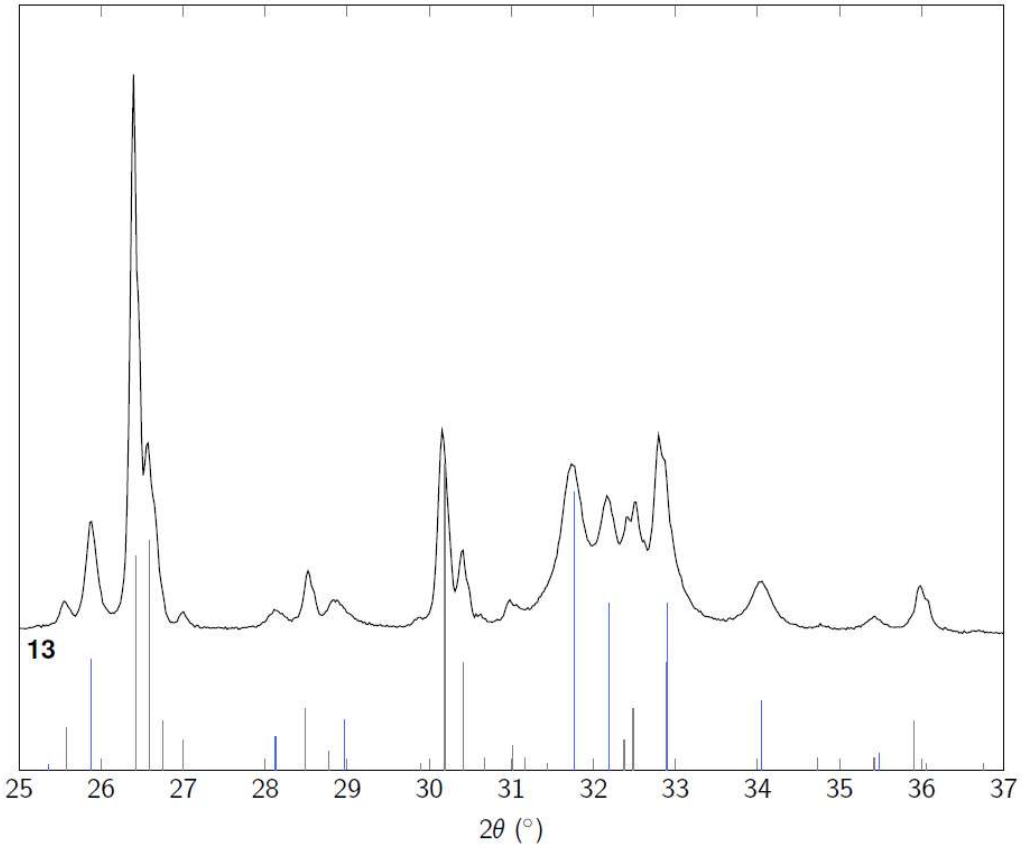

Figure S8. XRD patterns of the sample 13 prepared at pH 4.2 and 80 °C following the Ca → P synthesis route (Table 2) and position of the diffraction lines expected for DCPA (grey, ICDD reference card n° 00-009-0080) and for HAp (blue, ICDD reference card n° 00-009-043).

S9 - High magnification images of rod-like and platelet/ribbon-like crystallites

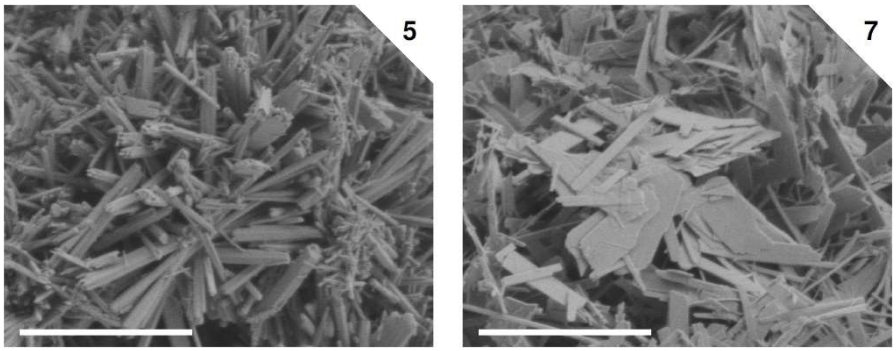

Figure S9. Scanning electron microscopy images of samples 5 and 7 prepared at pH 6.5 following the Ca → P and P → Ca routes, respectively. The numbers indicated on the top right corners of the images refer to as the sample references listed in Table 2. Scale bars: 2 µm.

S10 - Hexagonal section of samples 2 and 5

Transmission electron microscopy (TEM) observations were done on ultrathin cuttings of crystallites in order to visualize hexagonal sections of few rods (Table 2, samples 2 and 5). The sections were prepared as follows: a few milligrams of powder were embedding in a resin. Polymerization of the resin took place at 70 °C for 48 h, then the polymerized blocks were cut with a diamond knife in slices (around 70 nm in thickness). These slices were then deposited on copper grids covered with a carbon membrane layer. TEM images were taken on a JEOL-JEM2100Plus electron microscope operating at 200 keV (LaB_6 gun). For samples 2 and 5, crystallites with a more or less distorted hexagonal section are observed (Figure S10).

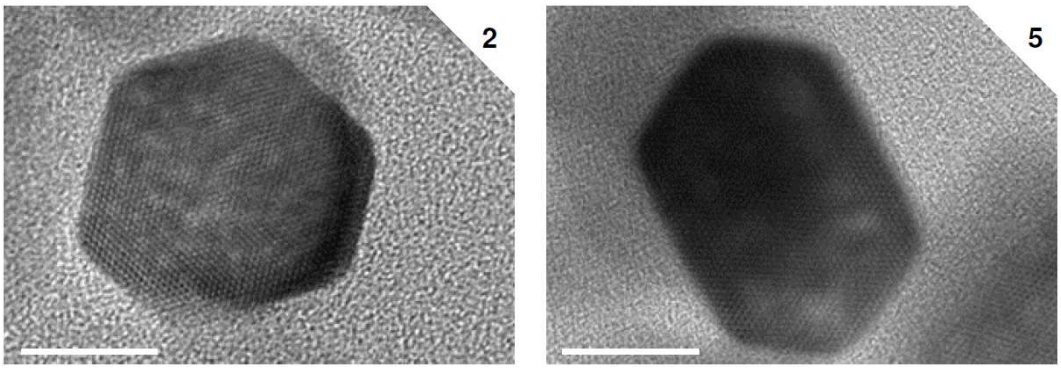

Figure S10. TEM images of hexagonal sections of rods from samples 2 and 5 prepared according to the P → Ca route at pH 9.0 and 6.5, respectively. The numbers indicated on the top right corners of the images refer to as the sample references listed in Table 2. Scale bars: 20 nm.

References

(1) Bandura, A. V.; Lvov, S. N. The Ionization Constant of Water over Wide Ranges of Temperature and Density. *J. Phys. Chem. Ref. Data* **2005**, *35*, 15–30.

(2) Emerson, K.; Russo, R. C.; Lund, R. E.; Thurston, R. V. Aqueous Ammonia Equilibrium Calculations: Effect of pH and Temperature. *J. Fish. Board Can.* **2011**.

(3) Blakeslee, K. C.; Condrate, R. A. Vibrational Spectra of Hydrothermally Prepared Hydroxyapatites. *J. Am. Ceram. Soc.* **1971**, *54*, 559–563.

(4) Stammeier, J. A.; Purgstaller, B.; Hippler, D.; Mavromatis, V.; Dietzel, M. In-Situ Raman Spectroscopy of Amorphous Calcium Phosphate to Crystalline Hydroxyapatite Transformation. *MethodsX* **2018**, *5*, 1241–1250.

(5) Fowler, B. O.; Marković, M.; Brown, W. Octacalcium Phosphate. 3. Infrared and Raman Vibrational Spectra. *Chem. Mater.* **1993**, *5*, 1417–1423.

(6) Xu, J.; Butler, I. S.; Gilson, D. F. R. FT-Raman and High-Pressure Infrared Spectroscopic Studies of Dicalcium Phosphate Dihydrate ($CaHPO_4 \cdot 2H_2O$) and Anhydrous Dicalcium Phosphate ($CaHPO_4$). *Spectrochim. Acta Part Mol. Spectrosc.* **1999**, *55*, 2801–2809.

(7) McDowell, H.; Gregory, T. M.; Brown, W. E. Solubility of $Ca_5(PO_4)_3OH$ in the System $Ca(OH)_2$-H_3PO_4-H_2O at 5, 15, 25, and 37 °C. *J. Res. Natl. Bur. Stand. Sect. Phys. Chem.* **1977**, *81A*, 273–281.

(8) Suchanek, K.; Bartkowiak, A.; Perzanowski, M.; Marszałek, M. From Monetite Plate to Hydroxyapatite Nanofibers by Monoethanolamine Assisted Hydrothermal Approach. *Sci. Rep.* **2018**, *8*.

(9) Chen, S.; Krumova, M.; Cölfen, H.; Sturm, E. V. Synthesis of Fiber-like Monetite without Organic Additives and Its Transformation to Hydroxyapatite. *Chem. Mater.* **2019**, *31* (5), 1543–1551.